Visualization of the aneurysm wall: a 7.0-tesla magnetic resonance imaging study

Kleinloog, Rachel ; Korkmaz, Emine ; Zwanenburg, Jaco J M ; Kuijf, Hugo J ; Visser, Fredy ; Blankena, Roos ; Post, Jan Andries ; Ruigrok, Ynte M ; Luijten, Peter R ; Regli, Luca ; Rinkel, Gabriel J E ; Verweij, Bon H

DOI: https://doi.org/10.1227/NEU.0000000000000559

Visualization of the Aneurysm Wall: A 7.0-Tesla Magnetic Resonance Imaging Study

Rachel Kleinloog, MD*
Emine Korkmaz, MSc‡
Jaco J.M. Zwanenburg, PhD§¶
Hugo J. Kuijf, PhD§
Fredy Visser¶||
Roos Blankena, BSc*#
Jan A. Post, PhD‡
Ynte M. Ruigrok, MD, PhD*
Peter R. Luijten, PhD¶
Luca Regli, MD, PhD**
Gabriel J.E. Rinkel, MD, FRCPE*
Bon H. Verweij, MD, PhD*

*Department of Neurology and Neurosurgery, Brain Center Rudolf Magnus, §Image Sciences Institute, and ¶Department of Radiology, University Medical Center Utrecht, Utrecht, the Netherlands; ‡Biomolecular Imaging, Department of Biology, Science Faculty, Utrecht University, Utrecht, the Netherlands; ||Philips Healthcare, Best, the Netherlands; #Faculty of Science and Technology, Department of Technical Medicine, University of Twente, Enschede, the Netherlands; **Department of Neurosurgery, University Hospital Zurich, Zurich, Switzerland

Correspondence:
Bon H. Verweij, MD, PhD,
Department of Neurology and Neurosurgery,
Brain Center Rudolf Magnus,
University Medical Center Utrecht,
Heidelberglaan 100, 3508 GA Utrecht,
Netherlands.
E-mail: bverweij@umcutrecht.nl

Received, February 5, 2014.
Accepted, July 16, 2014.
Published Online, September 24, 2014.

BACKGROUND: Risk prediction of rupture of intracranial aneurysms is poor and is based mainly on lumen characteristics. However, characteristics of the aneurysm wall may be more informative predictors. The limited resolution of currently available imaging techniques and the thin aneurysm wall make imaging of wall thickness challenging.

OBJECTIVE: To introduce a novel protocol for imaging wall thickness variation using ultra–high-resolution 7.0-Tesla (7.0-T) magnetic resonance imaging (MRI).

METHODS: We studied 33 unruptured intracranial aneurysms in 24 patients with a T1-weighted 3-dimensional magnetization-prepared inversion-recovery turbo-spin-echo whole-brain sequence with a resolution of 0.8 × 0.8 × 0.8 mm. We performed a validation study with a wedge phantom and with 2 aneurysm wall biopsies obtained during aneurysm treatment using ex vivo MRI and histological examination and correlating variations in MRI signal intensity with variations in actual thickness of the aneurysm wall.

RESULTS: In vivo, the aneurysm wall was visible in 28 of the 33 aneurysms. Variation in signal intensity was observed in all visible aneurysm walls. Ex vivo MRI showed variation in signal intensity across the wall of the biopsies, similar to that observed on the in vivo images. Signal intensity and actual thickness in both biopsies had a linear correlation, with Pearson correlation coefficients of 0.85 and 0.86.

CONCLUSION: Unruptured intracranial aneurysm wall and its variation in thickness can be visualized with 7.0-T MRI. Aneurysm wall thickness variation can now be further studied as a risk factor for rupture in prospective studies.

KEY WORDS: Aneurysm, Cerebrovascular disorders, Magnetic resonance imaging, Risk factor, Wall thickness

Neurosurgery 75:614–622, 2014 DOI: 10.1227/NEU.0000000000000559 www.neurosurgery-online.com

Risk prediction of rupture of intracranial aneurysms is based mainly on the size of the aneurysm, with large aneurysms more prone to bleeding.[1] Most unruptured aneurysms discovered incidentally or during screening are, however, small[2] with an inherently small risk of rupture.[3] Consequently, most small aneurysms are left untreated.[3] However, most ruptured aneurysms are small, which is explained by the relatively high prevalence of small unruptured aneurysms.[4,5] Therefore, better identification of rupture-prone aneurysms is needed to tailor preventive treatment to those aneurysms. So far, studies on risk factors for aneurysm rupture have focused on the aneurysm lumen. Characteristics of the aneurysm wall are probably more important for rupture assessment; thus, imaging of the aneurysm wall seems pivotal to improve risk assessment of aneurysms. Postmortem and intraoperative studies have shown that the aneurysm wall can be very thin (0.02-0.50 mm)[6] with variation in thickness.[7,8] The spatial resolution of the currently available imaging techniques, including 3.0-T magnetic resonance imaging (MRI),[9] is insufficient to image the thickness of such thin structures.[10,11] Although 7.0-T MRI enables imaging with increased signal-to-noise ratio and a higher spatial resolution, the resolution is still insufficient, given the typically very thin wall of aneurysms. When the vessel wall is of a similar size as or is smaller than the size of 1 voxel (resolution), partial volume effects occur, and traditional thickness measurements therefore overestimate the actual thickness. However, variation in thickness of the vessel wall will produce a variation in signal

intensity of the voxel, particularly when the signals of surrounding structures (blood on one side of the wall and cerebrospinal fluid on the other side) are low. We hypothesized that thickness variation in the aneurysm wall can be visualized as signal intensity variation with 7.0-T MRI. When a recently developed sequence in which blood and cerebrospinal fluid are black is used to image the intracranial arterial wall,[12] the signal intensity variations observed across the aneurysm wall should be reflecting the amount of aneurysm wall tissue in 1 voxel and thus the actual thickness variations of the wall. In the present study, we combined in vivo imaging with ex vivo validation experiments to investigate whether the aneurysm wall can be visualized on 7.0-T MRI and whether intensity variation indeed reflects variation in thickness of the aneurysm wall.

METHODS

Patient Selection

Patients with unruptured intracranial aneurysms were recruited through the neurological and neurosurgical outpatient clinic in our center between July 2011 and June 2013. Patients with contraindications for 7.0-T MRI (eg, claustrophobia, metal objects such as dental implants or prostheses in or on the body, clips or coils used for previous aneurysm treatment) were excluded, as were patients with underlying vascular malformations such as arteriovenous malformations. All patients participating in this study gave written informed consent, and this study was approved by the Institutional Review Board of our center.

In Vivo Imaging of the Aneurysm Wall

Imaging was performed on a 7.0-T MRI scanner (Philips Healthcare, Cleveland, Ohio) with a 32-channel SENSE receive head coil and a volume transmit coil (Nova Medical, Wilmington, Massachusetts). A T1-weighted 3-dimensional magnetization-prepared inversion-recovery turbo-spin-echo (further referred to as $MR_{in\ vivo}$) sequence with whole-brain coverage, as described previously[12] and developed to image the intracranial vessel wall, was used to image the aneurysm wall. Briefly, the scan parameters were as follows: field of view, 250 × 250 × 190 mm (foot to head × anterior to posterior × right to left); acquired resolution, 0.8 × 0.8 × 0.8 mm; repetition time/inversion time/echo time, 3952/1375/37 milliseconds; and a variable-reduced refocusing flip angle scheme. The sequence was fat-suppressed using a spectral attenuated inversion-recovery pulse with 220-millisecond inversion delay. Parallel imaging with 2-dimensional sensitivity encoding was used with an acceleration factor of 6 (2 × 3, anterior to posterior × right to left), yielding a scan duration of approximately 11 minutes. In each patient, the protocol also contained a time-of-flight sequence for anatomic depiction of the aneurysm. The parameters of the time-of-flight sequence were as follows: repetition time/echo time, 15/3.2 milliseconds; flip angle, 25°; field of view, 200 × 190 × 50 mm (anterior to posterior × right to left × foot to head); acquired resolution, 0.25 × 0.30 × 0.40 mm; and sensitivity encoding with an acceleration factor of 2.2 (in the right-to-left direction). The scan duration was approximately 9 minutes. One patient whose images were heavily affected by movement artifacts was excluded from further analysis, as was a second patient whose images were affected by local artifacts at the aneurysm location (resulting from a location close to the skull base).

Ex Vivo Imaging of the Aneurysm Wall

Ex Vivo Aneurysm Wall Biopsy Preparation

The aneurysm wall biopsies were obtained from 2 patients who underwent clipping of their unruptured aneurysm and participated in an aneurysm wall tissue collection study. The first patient (patient 1), a 66-year-old woman, had a middle cerebral artery aneurysm with a luminal diameter of 7 mm. The second patient (patient 2), a 56-year-old man, had a large, partially thrombosed middle cerebral artery aneurysm (luminal diameter, 25 mm). A part of the aneurysm fundus distal to the clip was excised when complete obliteration of the aneurysm was confirmed by the surgeon using visual inspection and intraoperative indocyanine green angiography. The excision was performed at a location convenient for the surgeon. After excision, the wall biopsy was immediately submerged into 4% paraformaldehyde fixative in 0.1 mol/L phosphate buffer (pH 7.4) for at least 1 hour at room temperature and stored at 4°C until further preparation. For MRI, the wall biopsies were rinsed in 0.1 mol/L phosphate buffer followed by gradual infiltration with 4% gelatin (in 0.1 mol/L phosphate buffer) at 37°C. Biopsies were then embedded in fresh 4% gelatin solution in a Petri dish and left at 4°C to solidify overnight, avoiding air bubbles. Before MRI, the Petri dishes containing the gelatin-embedded biopsies were submerged in Fomblin (Solvay Solexis, Bollate, Italy), a proton-free fluid without MRI signal, to prevent artifacts at the borders.

Ex Vivo MRI Protocol

The wall biopsies were scanned in a single session on the 7.0-T MRI using the same 32-channel head coil used for in vivo imaging. A sequence nearly identical to the in vivo sequence (further referred to as $MRI_{ex\ vivo\ 0.8\ mm}$) was used, with the following slight adjustments to the parameters for the ex vivo situation: The TI was lowered to 1100 milliseconds to null the signal from the gelatin. Because of the smaller size of the specimen, sensitivity-encoding acceleration was removed, and the field of view was reduced by a factor of 2 in the right-to-left direction and 3 in the anterior-to-posterior direction, which resulted in the same scan time, turbo spin-echo train, and resolution as in the in vivo protocol while avoiding potential sensitivity-encoding artifacts. We performed an additional scan with ultra–high resolution (0.18-mm isotropic voxels, further referred to as $MRI_{ex\ vivo\ 0.18\ mm}$), which was used only to align histology with the images from the $MRI_{ex\ vivo\ 0.8\ mm}$ scan. The scan parameters of the $MRI_{ex\ vivo\ 0.18\ mm}$ scan were described before,[13] and this scan had an acquisition time of >3 hours.

Histological Examination of Aneurysm Wall Biopsies

After MRI, the wall biopsies were put in a 37°C incubator to liquefy the gelatin before final rinsing in 0.1 mol/L phosphate buffer. Biopsies were further processed for histology using standard procedures and embedded in paraffin in the preferred orientations to imitate the original position of the biopsies during ex vivo MRI. Then, 4-μm-thick serial sections of each sample were cut with a microtome and mounted on glass slides for hematoxylin and eosin histological staining. The serial sections of both biopsies were imaged with a light microscope with × 4 objective (Provis AX70; Olympus), and a selection of 7 sections of each biopsy was made that was evenly distributed throughout the biopsy sample and was free of microtome cutting artifacts. A Nikon DXM1200 digital camera and Nikon ATC-1 software (Nikon Instruments Europe) were used to capture images of this selection of sections.

Selection of Corresponding Cross Sections of the Aneurysm Wall Biopsies

For each aneurysm wall biopsy, the 7 images of the selected sections of the wall were compared with 2-dimensional transversal oriented slices of the wall as obtained with the ultra–high-resolution $MRI_{ex\ vivo\ 0.18\ mm}$. From each biopsy, the cross section that showed the best alignment on the basis of its anatomy between histology and the $MRI_{ex\ vivo\ 0.18\ mm}$ was selected by visual inspection. This was done by taking into account the order of the sections of both MR slices and histological sections, thereby ensuring that the histological section and the MR slice represented the same location in the tissue. After identification of the correct slice of the $MRI_{ex\ vivo\ 0.18\ mm}$, we selected the slice with the same orientation and location as the $MRI_{ex\ vivo\ 0.8\ mm}$.

Measurement of Signal Intensity Variation on MRIs

Variation in signal intensity in the $MRI_{ex\ vivo\ 0.8\ mm}$ slice was visualized with an intensity curve showing the changes in signal intensity in a path manually drawn across the center of the aneurysm wall using MeVisLab (MeVis Medical Solutions AG, Bremen, Germany).[14] A local signal averaging was applied to correct for drawing inaccuracies. The signal intensities across the path were plotted to obtain a profile curve of the variation in signal intensity across the wall.

Measurement of Actual Thickness Variation on Histological Sections

Actual thickness was measured on the histological sections using Matlab (Mathworks, Natick, Massachusetts), as follows: Segmentation of the tissue was performed, and the centerline of the tissue was computed. Measurements were performed perpendicular to this centerline to measure full thickness of the wall at multiple points across this line. The measurements were plotted to obtain a curve of the variation in actual thickness across the wall. The histological sections of biopsy 1 were all suitable for this analysis, but because there was little difference in the anatomy of these sections, we used the middle section for correlation analysis. For biopsy 2, only a part of the selected section was suitable for the correlation analysis. Because of intraoperative cutting damage, thickness measurements were not possible in the other part or in the other 6 sections of biopsy 2. In addition, histopathological examination of the selected cross sections was performed.

Correlation Analysis of Signal-Intensity Curves and Actual Thickness Curves

The curves of the variation in signal intensity and actual thickness were normalized between 0 and 1. The signal-intensity curve was rescaled to have the same physical length as the histological section. The signal-intensity curve was cropped to remove the extreme ends where the MRI signal started to diminish. Then, the 2 curves were aligned by maximizing the cross-correlation of the 2 curves with Matlab. After aligning the signal-intensity curve and the actual thickness curve, we correlated both data sets and calculated the Pearson correlation coefficient. Slight tilting of the biopsies while being processed for histological examination might have compromised accurate matching with the corresponding MRI slice at the edges of the tissue. Therefore, for 1 biopsy (biopsy 1), we also compared measurements from the MRI and histological examination excluding the edges.

Wedge Phantom Imaging

To illustrate the basic principle that signal intensity produced by partial volume effects is related to the size of the object, we performed imaging on a wedge phantom. By placing 1 end of a 6-mm-thick, 10-cm-long polymethyl methacrylate sheet on a polytetrafluorethylene strip with a thickness of 2.3 mm in a box filled with water, we created a wedge phantom with increasing thickness ranging from 0 to 2.3 mm. This phantom was scanned with the same protocol as used for the in vivo aneurysm imaging. The signal intensity variation was measured in the same way as in the ex vivo experiment with MeVisLab. Because of the large size of the phantom, we corrected the signal intensities for inhomogeneity induced by the receive coil sensitivity and the transmit field inhomogeneity. This was done by measuring a reference intensity profile of the water above the polymethyl methacrylate sheet (without partial volume effects) and dividing the intensity profile from the wedge phantom by the reference profile.

RESULTS

In Vivo Imaging of the Aneurysm Wall

In vivo images of the aneurysm wall on 7.0-T MRI were obtained in 24 patients with 33 unruptured aneurysms. The size (largest luminal diameter) of the aneurysms varied from 2 to 25 mm. In 28 of the 33 aneurysms, the wall was visible because it exhibited a higher signal than cerebrospinal fluid and blood (example shown in Figure 1). The intensity of the wall is equal to the intensity of brain tissue and intraluminal thrombus; therefore, the parts of the wall aligning the brain or intraluminal thrombus could not be assessed. Four aneurysms were completely enclosed by surrounding tissue (brain or dura), and in one of the aneurysms, the lumen was almost completely thrombosed. In these cases, the aneurysm wall could not be distinguished at all (Figure 2). In all of the 28 aneurysms visible on the $MR_{in\ vivo}$ images, we detected variations in signal intensity across the aneurysm wall (Figure 2).

Ex Vivo Imaging of the Aneurysm Wall

$MR_{ex\ vivo\ 0.8\ mm}$ images of the 2 aneurysm wall biopsies showed a hyperintense signal similar to that observed on the $MR_{in\ vivo}$ images. When a 3-dimensional image reconstruction of the aneurysm wall was visually compared with a macroscopic picture of the biopsy, the pattern of variation in signal intensity was similar to that of the variation in wall thickness (Figure 3). The actual thickness of the aneurysm wall, as measured by histological examination, ranged between 0.2 and 0.6 mm in biopsy 1 and between 0.2 and 1.6 mm in biopsy 2. Histopathological examination of the thinnest part of biopsy 1 showed a remarkably hypocellular wall, consisting mainly of collagen, with a complete absence of endothelial lining. The thicker part showed minor hyperplasia of the intimal layer, the presence of inflammatory cells, an abundance of collagen, and an intact endothelial lining. An examination of the thick part of biopsy 2 showed a hypercellular wall without distinguishable layers with infiltration of inflammatory cells and the presence of thrombosis. Degeneration of the extracellular matrix was found, as were spindle-shaped smooth muscle cells. Some vaso vasorum were identified in the abluminal layer. The thinner parts of this biopsy were less cellular and showed disorganized collagen.

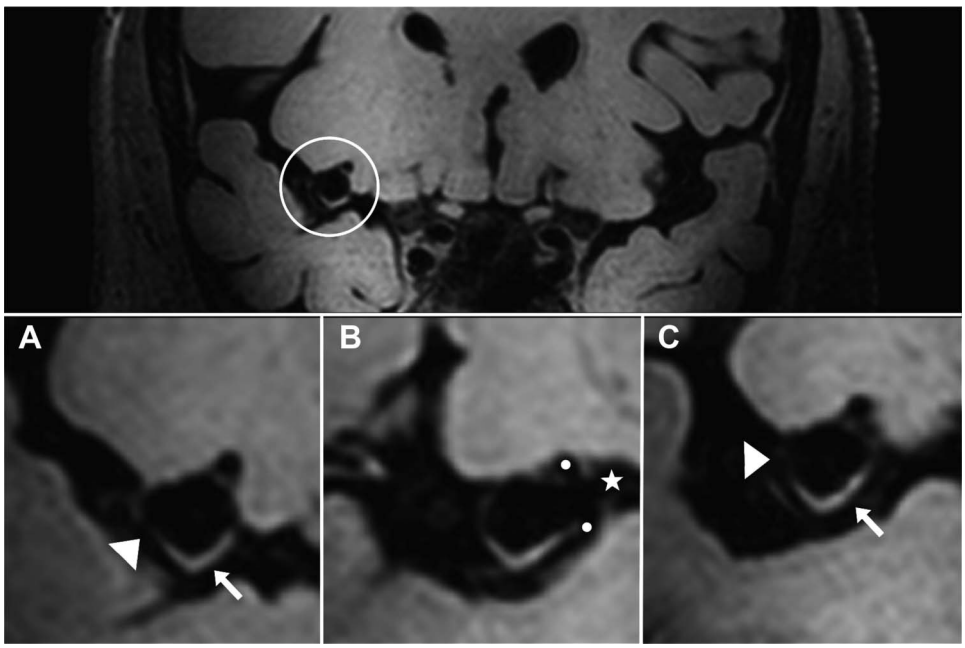

FIGURE 1. *In vivo imaging of an aneurysm wall on 7.0-T magnetic resonance imaging. In vivo images of the wall of a right middle cerebral artery aneurysm with an intraluminal diameter of 7 mm (**top**, coronal view; aneurysm marked with a circle) show variation in signal intensity across the wall. **A**, magnification of the **top** panel showing apparently thin (low signal intensity, arrowhead) and thick (high intensity, arrows) portions of the wall. **B**, oblique cross section in which the lumen of the parent artery (M1 segment of the middle cerebral artery, star) and the branching arteries (M2 segments of the middle cerebral artery, dots) are visible. **C**, another oblique cross section of the aneurysm wall, confirming that the aneurysm is not in contact with surrounding brain tissue with its apparently thick part of the wall (arrow).*

Correlation Analysis

The corresponding $MR_{ex\ vivo\ 0.8\ mm}$ images and the histological sections selected for correlation analysis by using $MR_{ex\ vivo\ 0.18\ mm}$ images are shown in Figure 4. The variation in actual wall thickness correlated with the variation in signal intensity of the wall on MRI (Figure 5). For both biopsies, we found a linear correlation between signal intensity and actual thickness (Pearson correlation coefficient: biopsy 1, 0.85; and biopsy 2, 0.86; Figure 5). When only the middle part of biopsy 1 was analyzed, the Pearson correlation coefficient increased to 0.97 (Figure 5A2).

Wedge Phantom Imaging

The results of the wedge phantom imaging showed that signal intensity increased linearly with thickness of the phantom until reaching a plateau at the point where the phantom size was larger than the voxel size of the sequence (Figure 6).

DISCUSSION

The present study shows that 7.0-T MRI can image intracranial aneurysm walls and assess variation in aneurysm wall thickness.

This is the first study confirming with a wedge phantom and histology data that in vivo imaging of aneurysm wall thickness variation is possible. Previously, 1 study described the imaging of unruptured aneurysm walls with a double-inversion recovery black-blood sequence on 1.5-T MRI with an in-plane resolution of 0.48×0.58 mm.[10] Spatial variations in thickness of the wall were observed, as in our study. Thickness of the wall was measured on MRI, and a mean thickness of 0.46 mm (SD, 0.05 mm) was found for the dome portion of the aneurysms. However, the method used in that study was noted to have several limitations,[11] which included a 3-mm slice thickness that results in large partial volume effects with seeming thickness variations when the orientation of the wall changes with respect to the orientation of the long anisotropic voxels. In addition, histological verification of the MRI measurements was lacking. In our study, we refrained from measuring wall thickness on in vivo MRIs because of partial volume effects; instead, we focused on finding an alternative method. We showed that instead of measuring actual thickness, it is possible to infer thickness variations, and we validated our findings with both a wedge phantom and an ex vivo study. Furthermore, because we used isotropic voxels instead of a high in-plane resolution, the orientation of the vessel wall with respect to the image plane has only a limited influence on the signal intensity. To perform actual thickness measurements of the aneurysm wall on MRI, at least 2 full voxels without partial

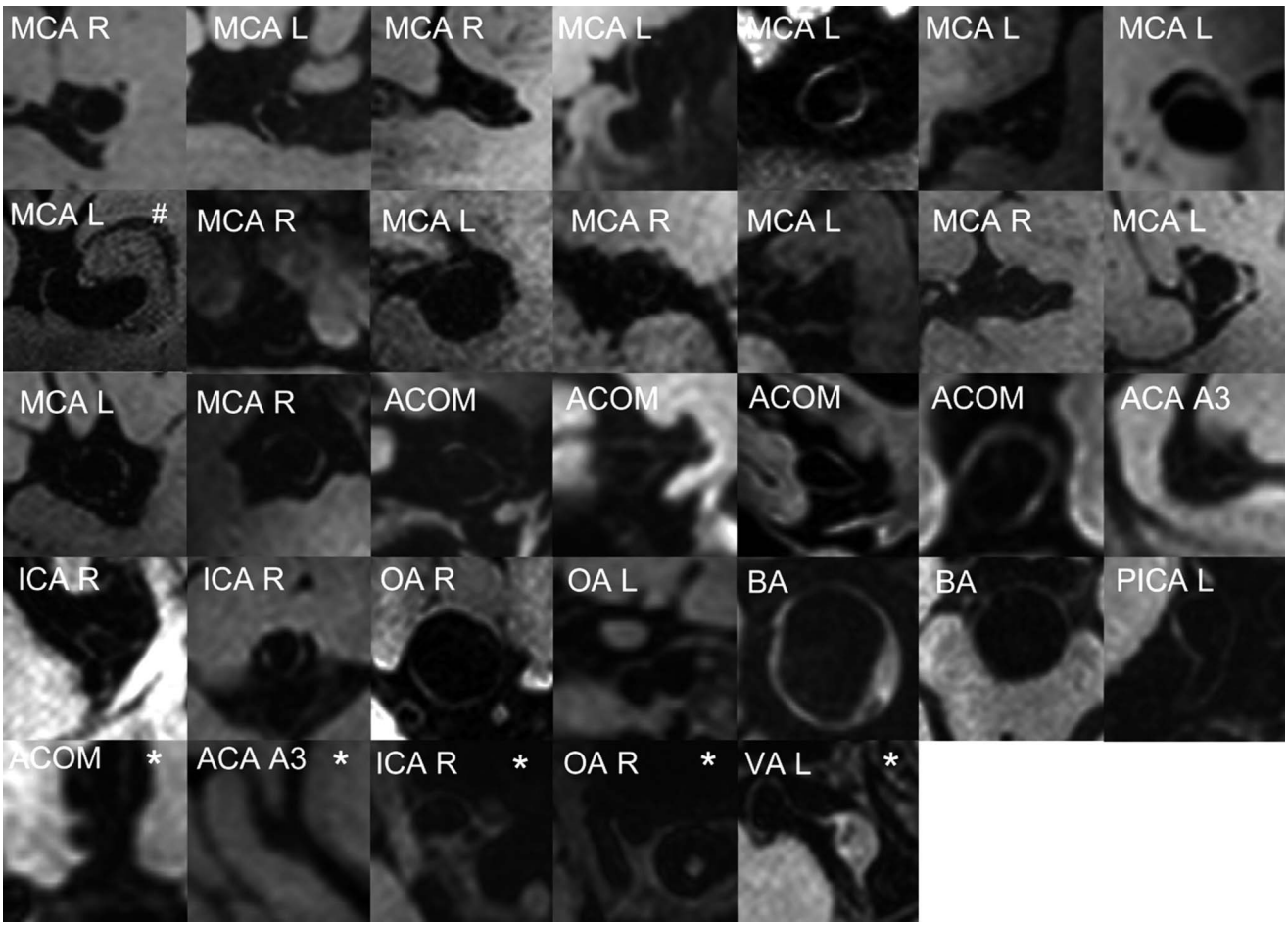

FIGURE 2. *Overview of in vivo aneurysm wall imaging on 7.0-T magnetic resonance imaging of all 33 unruptured intracranial aneurysms. Locations of the aneurysms are indicated. A partially thrombosed aneurysm is indicated with a hashtag (#). An asterisk (*) indicates the aneurysms in which we were unable to assess variations in signal intensity of the wall owing to their embedment in surrounding tissue or the presence of intraluminal thrombus. ACA A3, pericallosal artery; ACOM, anterior communicating artery; BA, basilar artery; ICA, internal carotid artery; MCA, middle cerebral artery; OA, ophthalmic artery; PICA, posterior inferior cerebellar artery; VA, vertebral artery.*

volume effects should represent the wall.[15] This would, for example, require an effective isotropic resolution of 0.1 mm for imaging an aneurysm wall thicker than 0.2 mm. Even with advanced imaging on 7.0-T MRI, this is not feasible in vivo. Neither is this expected to be feasible on machines with stronger magnets in the near future.

Imaging with 3-dimensional T1-weighted magnetization-prepared inversion-recovery turbo-spin-echo sequence on 7.0-T MRI visualized the aneurysm wall in >80% of the aneurysms and showed variation in signal intensity, reflecting variation in aneurysm wall thickness. Using a wedge phantom, we demonstrated the principle that thickness variation in a sheet/structure with subvoxel thickness can be inferred from variation in signal intensity when the signal intensities of surrounding tissues are suppressed. In aneurysms, this principle would hold only when the lumen of the aneurysm contains at least 2 voxels (to ensure that partial volume effects of opposite walls occur in different voxels), which would mean that aneurysms should have a diameter >3 mm. In theory, the principle that thickness variation can be inferred from variation in signal intensity would fail when the variation in composition of the wall influences the variation in intensity on MRI. The histopathological examination of the ex vivo biopsies showed a variable composition throughout the wall. However, the results of the correlation analysis of the 2 biopsies strongly suggest that, even in the presence of a variable wall composition, signal intensity reflects thickness variation for the sequence that was used in this study. This might be explained by the low contrast that is obtained with the slightly T1-weighted sequence used to image the aneurysm wall (eg, gray and white matter have approximately the same intensity).

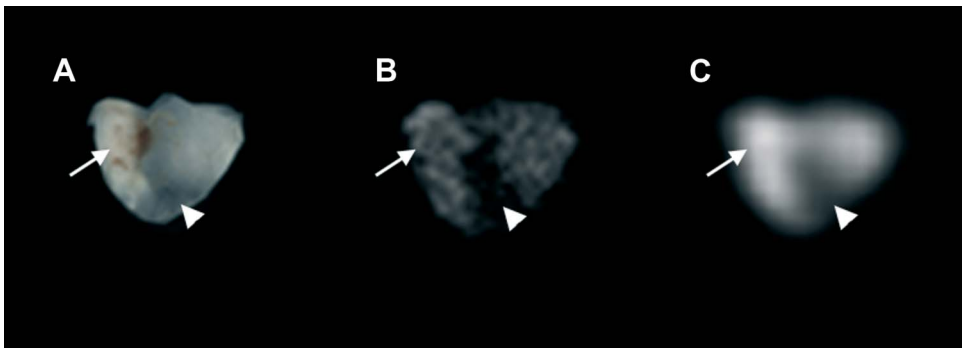

FIGURE 3. *Ex vivo imaging of the aneurysm wall. Image showing the visual correlation between signal intensity and actual thickness in wall biopsy 1. The part of the wall assumed to be thick on subsequent images is indicated with an arrow, and the thin part of the wall is indicated with an arrowhead.* **A**, *macroscopic picture of the entire biopsy in gelatin.* **B**, *screenshot of a 3-dimensional maximum-intensity projection of the 0.18-mm-resolution magnetic resonance images (MRIs) of the entire biopsy.* **C**, *screenshot of a 3-dimensional maximum-intensity projection of the ex vivo MRIs obtained with the 0.8-mm-resolution vessel wall sequence.*

The description of the histopathology of the different parts of the wall of the 2 biopsies included in our ex vivo validation experiment resembles the descriptions of each of the 4 histological wall types previously described in saccular aneurysms,[16] which are likely to reflect consecutive stages of wall degeneration proceeding to rupture. This suggests that these 2 biopsies are representative of aneurysms with wall compositions in any of the 4 consecutive stages proceeding to rupture and that therefore our method should be applicable to a large range of aneurysms with different histological wall types.

Limitations

Further studies should take into account some limitations of the imaging technique. First, pulsation of the aneurysm during the heart cycle in the in vivo situation can lead to blurring and signal loss of the wall, which would affect the apparent thickness. Therefore, the

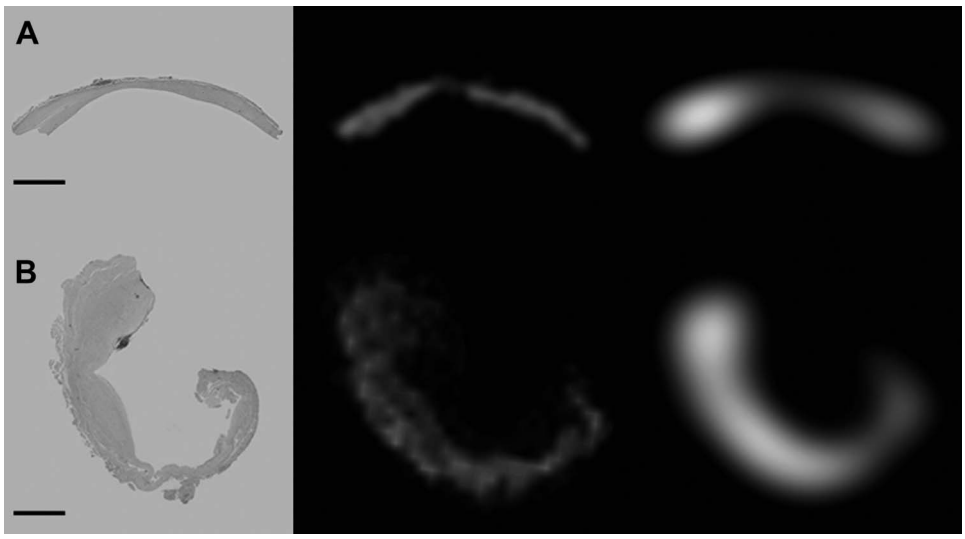

FIGURE 4. *Corresponding cross sections of the 2 wall biopsies selected for the ex vivo validation study.* **A**, *selected cross section of a middle cerebral artery aneurysm wall (wall biopsy 1).* **B**, *selected cross section of a middle cerebral artery aneurysm wall (wall biopsy 2). A slight change in configuration of biopsy 2 occurred because of a collapse of the tissue during paraffin embedment. From left to right: histological section (scale bar = 1 mm), slice of the 0.18-mm-resolution magnetic resonance image (MRI) used for alignment of the MRIs with histology, and the corresponding slice of the 0.8-mm-resolution MRI.*

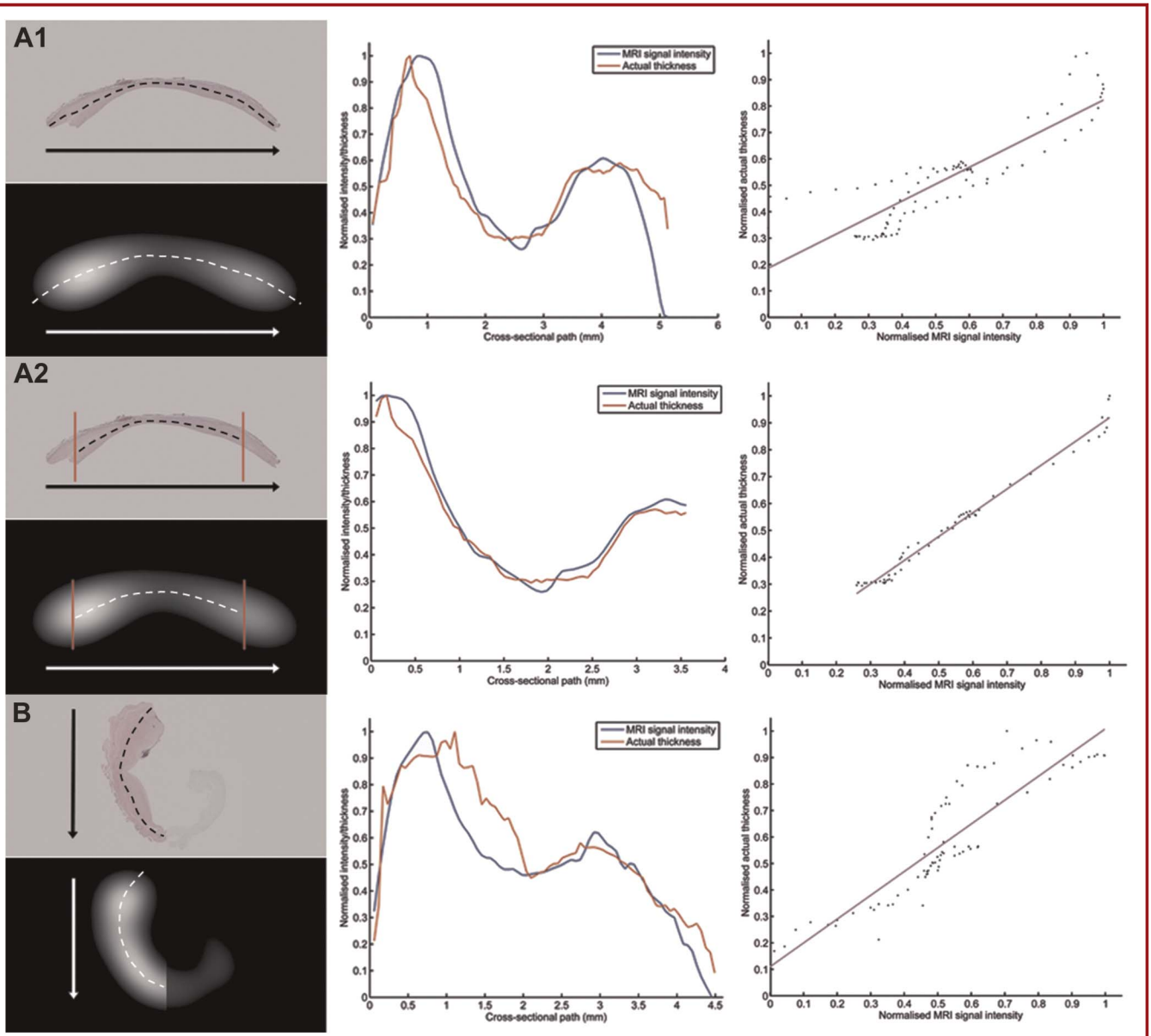

FIGURE 5. *Correlation of signal intensity variation and actual thickness variation in the aneurysm wall biopsies. From left to right: direction of the path through the center of the tissue in the histological section (***top***) and in the magnetic resonance imaging slice (***bottom***), curves of signal intensity (blue) and actual thickness (red) after normalization, and correlation between signal intensity and actual thickness.* **A1***, correlation in wall biopsy 1;* **A2***, correlation in the middle part of the tissue of biopsy 1. Red lines in the* **left** *panel indicate the selected region (representing the region between the peaks in intensity/thickness).* **B***, correlation in wall biopsy 2. We excluded a part of the histological section (transparent part) of wall biopsy 2 from the measurement because intraoperative cutting damaged the tissue and a thickness measurement was not possible in that part.*

pulsation of the aneurysm should be assessed in a separate scan to exclude this as a confounding factor. Second, the signal of the aneurysm wall is equal to that of brain tissue; therefore, the parts of the wall aligning the brain cannot be taken into account is the assessment of thickness variation as a risk factor for rupture. It is unclear how this will influence the future analyses because it was only suggested that ruptured aneurysms are more often in contact with surrounding anatomic structures than unruptured aneurysms.[17] Third, intraluminal thrombus has approximately the same signal intensity as the aneurysm wall, and its presence may confound the assessment of the thickness variations in the wall. However, an intraluminal thrombus can easily be identified on the

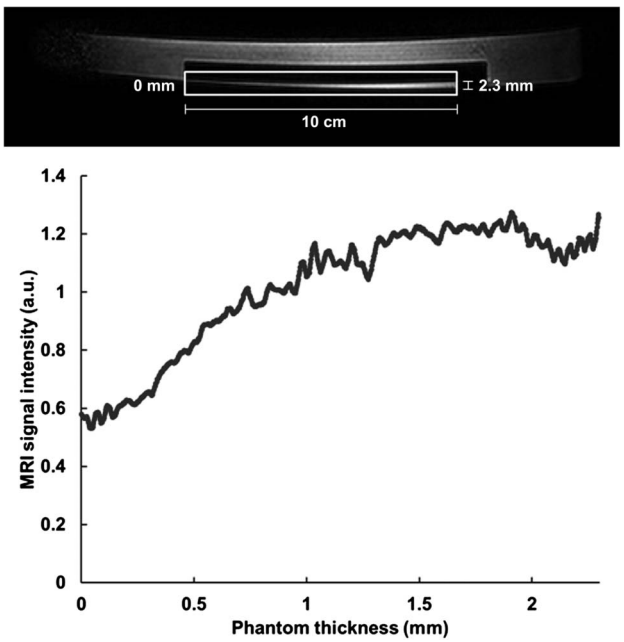

FIGURE 6. *Imaging of a wedge phantom to illustrate that signal intensity produced by partial volume effects is related to the thickness of the object.* **Bottom**, *curve of the magnetic resonance imaging signal intensity of the wedge phantom ranging in size from 0 to 2.3 mm, corrected for the inhomogeneity of the image intensity.* **Top**, *the image obtained when the polymethyl methacrylate wedge phantom (length, 10 cm) was scanned in a box with water. The water has a hyperintense signal, whereas the polymethyl methacrylate has no signal. The white box indicates the wedge on which the signal intensity measurements were performed (results of this analysis are shown in the* **bottom**). *The thickness range of the wedge is indicated. The image of the phantom is curved because of imperfect B0 shimming.*

time-of-flight sequence because it exhibits a lower signal than the hyperintense aneurysm lumen and the surrounding brain tissue. The information obtained with a time-of-flight sequence should therefore be taken into account in analyses of the aneurysm wall with MRI. Fourth, we used fat saturation on the T1-weighted 3-dimensional magnetization-prepared inversion-recovery turbo-spin-echo sequence to decrease the influence of water-fat shift on the images. When fat saturation is used, the signal intensity of the wall might decrease when fat is present, which would therefore influence the thickness variation measurement. However, the accumulation of lipids is thought to be limited and to occur mainly in macrophages that have infiltrated the wall.[18] These macrophages have a scattered distribution throughout the wall, and lipids are not accumulated in a lipid core underlying the fibrous cap of a vulnerable plaque, as is known to be the case in an extracranial atherosclerotic lesion. Therefore, we do not think that the use of fat suppression significantly influenced our results. However, future studies should elucidate the role of fat deposition in the aneurysm wall and its influence on imaging of the wall. Finally, the clinical availability of 7.0-T MRI is limited.

CONCLUSION

Unruptured aneurysms have a prevalence of 3% and are increasingly discovered by screening or as an incidental finding on imaging studies performed to diagnose or exclude a variety of cranial diseases.[2] Consequently, neurologists and neurosurgeons are frequently confronted with patients seeking advice about whether to undergo preventive treatment of their aneurysm. The answer to this question is currently based on risk factors with a limited predictive value.[1] Therefore, the need for new risk factors for rupture is great. Our study offers a new tool to study aneurysm wall thickness variation, which might be a possible risk factor for rupture, although it is still unclear whether a thin, a thick, or an irregular wall thickness is associated with rupture. The next step is to develop a standardized method in which aneurysm wall thickness variations can be quantified. Thereafter, follow-up studies assessing variation in wall thickness as a risk factor for rupture can be started in patients.

Disclosures

Dr Kleinloog and E. Korkmaz were supported by a Focus en Massa cardiovascular research grant from the Utrecht University, Utrecht, the Netherlands. Dr Ruigrok was supported by a NOW-VENI grant from the Netherlands Organization for Scientific Research (NOW; project No. 91610016). Dr Luijten serves as chief scientific officer for the Center for Translational Molecular Medicine. F. Visser is an employee of Philips Healthcare, Best, the Netherlands. The other authors have no personal, financial, or institutional interest in any of the drugs, materials, or devices described in this article.

REFERENCES

1. Wermer MJ, van der Schaaf IC, Algra A, Rinkel GJ. Risk of rupture of unruptured intracranial aneurysms in relation to patient and aneurysm characteristics: an updated meta-analysis. *Stroke*. 2007;38(4):1404-1410.
2. Vlak MH, Algra A, Brandenburg R, Rinkel GJ. Prevalence of unruptured intracranial aneurysms, with emphasis on sex, age, comorbidity, country, and time period: a systematic review and meta-analysis. *Lancet Neurol*. 2011;10(7):626-636.
3. Wiebers DO, Whisnant JP, Huston J III, et al. Unruptured intracranial aneurysms: natural history, clinical outcome, and risks of surgical and endovascular treatment. *Lancet*. 2003;362(9378):103-110.
4. Forget TR Jr, Benitez R, Veznedaroglu E, et al. A review of size and location of ruptured intracranial aneurysms. *Neurosurgery*. 2001;49(6):1322-1325.
5. Inagawa T. Size of ruptured intracranial saccular aneurysms in patients in Izumo City, Japan. *World Neurosurg*. 2010;73(2):84-92.
6. Suzuki J, Ohara H. Clinicopathological study of cerebral aneurysms: origin, rupture, repair, and growth. *J Neurosurg*. 1978;48(4):505-514.
7. Inagawa T, Hirano A. Autopsy study of unruptured incidental intracranial aneurysms. *Surg Neurol*. 1990;34(6):361-365.
8. Kadasi LM, Dent WC, Malek AM. Cerebral aneurysm wall thickness analysis using intraoperative microscopy: effect of size and gender on thin translucent regions. *J Neurointerv Surg*. 2013;5(3):201-206.
9. Swartz RH, Bhuta SS, Farb RI, et al. Intracranial arterial wall imaging using high-resolution 3-Tesla contrast-enhanced MRI. *Neurology*. 2009;72(7):627-634.
10. Park JK, Lee CS, Sim KB, Huh JS, Park JC. Imaging of the walls of saccular cerebral aneurysms with double inversion recovery black-blood sequence. *J Magn Reson Imaging*. 2009;30(5):1179-1183.
11. Steinman DA, Antiga L, Wasserman BA. Overestimation of cerebral aneurysm wall thickness by black blood MRI? *J Magn Reson Imaging*. 2010;31(3):766.
12. van der Kolk AG, Hendrikse J, Brundel M, et al. Multi-sequence whole-brain intracranial vessel wall imaging at 7.0 Tesla. *Eur Radiol*. 2013;23(11):2996-3004.

13. Korteweg MA, Zwanenburg JJ, Hoogduin JM, et al. Dissected sentinel lymph nodes of breast cancer patients: characterization with high-spatial-resolution 7-T MR imaging. *Radiology*. 2011;261(1):127-135.
14. Ritter F, Boskamp T, Homeyer A, et al. Medical image analysis. *IEEE Pulse*. 2011; 2(6):60-70.
15. Shannon C. Communication in the presence of noise. *Proc Inst Radio Eng*. 1949; 37:10-21.
16. Frösen J, Piippo A, Paetau A, et al. Remodeling of saccular cerebral artery aneurysm wall is associated with rupture: histological analysis of 24 unruptured and 42 ruptured cases. *Stroke*. 2004;35(10):2287-2293.
17. San Millán Ruíz D, Yilmaz H, Dehdashti AR, Alimenti A, de Tribolet N, Rüfenacht DA. The perianeurysmal environment: influence on saccular aneurysm shape and rupture. *AJNR Am J Neuroradiol*. 2006;27(3):504-512.
18. Frösen J, Tulamo R, Paetau A, et al. Saccular intracranial aneurysm: pathology and mechanisms. *Acta Neuropathol*. 2012;123(6):773-786.

Acknowledgments

We thank M.A. van Es, MD, PhD, for valuable comments on a previous version of this manuscript. We sincerely acknowledge the use of MeVisLab.

COMMENT

This is an observational study on the use of an optimized magnetic resonance imaging (MRI) pulse sequence at high magnetic field strength (7 T) to image the vessel wall of cerebral aneurysms. Studying 33 unruptured aneurysms in vivo, the authors found that there is spatial variability in aneurysm wall MRI signal intensity. On the basis of theoretical considerations, a phantom study, and 2 cases with histopathological correlation, the authors provide preliminary evidence that MRI can demonstrate spatial variability in aneurysm wall thickness. The ultimate goal is to develop a new means of predicting aneurysm rupture risk. There is a wealth of research on the hemodynamics of cerebral aneurysms, but there is a relative paucity of investigation into imaging aneurysm wall characteristics in vivo. This is certainly a field worthy of further study.

Daniel M. Mandell
Toronto, Ontario, Canada